Comput Mech (2005) 36: 117–128
DOI 10.1007/s00466-004-0644-3

ORIGINAL PAPER

Xianwu Ling · H. P. Cherukuri · R. G. Keanini

A modified sequential function specification finite element-based method for parabolic inverse heat conduction problems

Received: 24 October 2003/ Accepted: 18 April 2004 / Published online: 25 January 2005

Abstract A method for enhancing the stability of parabolic inverse heat conduction problems (IHCP) is presented. The investigation extends recent work on non-iterative finite element-based IHCP algorithms which, following Beck's two-step approach, first derives a discretized standard form equation relating the instantaneous global temperature and surface heat flux vectors, and then formulates a least squares-based linear matrix normal equation in the unknown flux. In the present study, the non-iterative IHCP algorithm is stabilized using a modified form of Beck's sequential function specification scheme in which: (i) inverse solution time steps, Δt, are set larger than the data sample rate, $\Delta\tau$, and (ii) future temperatures are obtained at intervals equal to $\Delta\tau$. These modifications, contrasting with the standard approach in which the computational, experimental, and future time intervals are all set equal, are designed respectively to allow for diffusive time lag (under the typical circumstance where $\Delta\tau$ is smaller than, or on the order of the characteristic thermal diffusion time scale), and to improve the temporal resolution and accuracy of the inverse solution. Based on validation tests using three benchmark problems, the principle findings of the study are as follows: (i) under dynamic surface heating conditions, the modified and standard methods provide comparable levels of early-time resolution; however, the modified technique is not subject to over-damped estimation (as characteristic of the standard scheme) and provides improved error suppression rates, (ii) the present method provides superior performance relative to the standard approach when subjected to data truncation and thermal measurement error, and (iii) in the nonlinear test problem considered, both approaches provide comparable levels of performance. Following validation, the technique is applied to a quenching experiment and estimated heat flux histories are compared against available analytical and experimental results.

Keywords Heat conduction · Inverse methods · Heat transfer coefficient · Finite element method · Sequential function specification

R. G. Keanini (✉)
Mechanical Engineering, UNC-Charlotte,
9201 University City Blvd,
Charlotte, NC 28223-0001, USA
Tel.: 704-687-4158
Fax: 704-687-2352
E-mail: rkeanini@uncc.edu

X. Ling · H. P. Cherukuri · R. G. Keanini (✉)
Department of Mechanical Engineering and Engineering Science
The University of North Carolina at Charlotte Charlotte,
NC 28223-0001, USA

Nomenclature

a	temperature coefficient in linear expansions for k and c,Test Case 3
$\mathbf{A}$, $\mathbf{B}$, $\mathbf{C}$, $\mathbf{D}$	coefficient matrices in standard form equation
c	specific heat
$\mathbf{c}^{(\mathbf{m})}$	global vector produced by condensation, evaluated at the *mth* future time
$\mathbf{f}$	global force vector
$\mathbf{f}^{(\mathbf{m})}$	global force vector evaluated at the *mth* future time
$h; h^{n+1}$	estimated instantaneous convective heat transfer coefficient
k	thermal conductivity
$\mathbf{K}$	global stiffness matrix
L	thickness of test specimen; depth of embedded temperature probe
$\mathbf{M}$	global mass matrix
N_i	*ith* interpolation function
$\mathbf{n}$	surface unit normal
q_c	magnitude of impulsively imposed heat flux (Test Case 1)
q^+	dimensionless estimated surface heat flux $(= q^n/q_c)$
$\mathbf{q}$	global vector of surface heat fluxes
$\tilde{\mathbf{q}}^{n+1}$	heat flux parameter vector evaluated at t^{n+1}

r	number of future times used in the standard method $[(r-1)\beta = R]$
R	number of future times used in present method
S^{n+1}	instantaneous least square error norm (at t^{n+1})
t	time
t^+	dimensionless time $(= \alpha t/L^2)$
δt	computational time step (for inverse solution)
δt^+	dimensionless computational time step $(= \alpha \delta t/L^2)$
δt_f	future time step size
$t^{(m)}$	the *mth* future time
$\mathbf{U}^{(\mathbf{m})}$	global matrix in standard form equation $(= [\boldsymbol{M} + \Delta t^{(m)} \boldsymbol{K}]^{-1})$
x	x-coordinate
x^+	dimensionless x-coordinate $(= x/L)$
u	Kirchoff transformation variable, Test Case 3
$\mathbf{X}$	position vector
$\mathbf{X}^{(\mathbf{n+1})}$	sensitivity matrix, evaluated at $\boldsymbol{t}^{n+1}$
$\tilde{\mathbf{Y}}^{(m)}$	vector of measured temperatures, obtained at future time $t^{(m)}$
α	thermal diffusivity
β	time-scale multiplication factor $(= \Delta t/\Delta\tau)$
Γ_1, Γ_2	surface regions where temperature and heat flux boundary conditions are applied, respectively
Γ_e	finite element boundary
$\boldsymbol{\theta}$	computed temperature field
θ_∞	ambient temperature
$\boldsymbol{\theta}_o$	initial temperature distribution
$\tilde{\boldsymbol{\theta}}^{(m)}$	vector of computed measurement site temperatures, obtained at future time $t^{(m)}$
ρ	density
$\Delta\tau$	sample time step
$\Delta\tau^+$	dimensionless sample time step $(= \alpha\Delta\tau/L^2)$
τ_D	thermal diffusion time scale between surface and embedded probe

Superscripts and overhead marks

(m)	future time index
$n, n+1$	time indices
$+$	dimensionless quantity
$\tilde{\cdot}$	reduced global matrix

Subscripts

o property evaluated at reference temperature θ_o

1 Introduction

The classical inverse heat conduction problem (IHCP) uses one or more temperature measurements taken from the interior of a body to estimate an unknown, typically time-varying surface heat flux distribution. The problem arises in a variety of applications, some of the more interesting of which are highlighted by Beck et al. [1] and Özisik and Orlande [2]. Over approximately 40 years of development, numerous methods have been proposed for treating the IHCP; comprehensive reviews of the literature can be found in Beck et al. [1], Özisik and Orlande [2], Tikhonov and Arsenin [3], Kurpisz and Nowak [4], Hensel [5], Murio [6], and Alifanov [7]. Applications, illustrating a variety of methods, are presented in Zabaras et al. [8], Delaunay et al. [9], Woodbury et al. [10], and Orlande at al. [11].

This article continues and extends recent work [12] on non-iterative methods for the IHCP. The technique developed in the first study, applicable to a broad class of parabolic inverse heat transfer problems in which a surface heat flux (or temperature) history is sequentially estimated given a known initial thermal state and limited subsequent thermal measurements, was guided by a generic, two-part strategy first described by Beck et al. [1]. In Beck's approach, the direct heat transfer model (describing conductive heat transfer in the body of interest) is used to first derive a linear (or in nonlinear problems, a quasilinear), discretized system of equations relating the instantaneous global temperature vector, $\boldsymbol{\theta}^{n+1}$, to the instantaneous vector of unknown surface heat fluxes $\mathbf{q}^{\mathbf{n+1}}$. The resultant *standard form equation*, which can be stated in generic form as

$$\mathbf{A}\dot{\boldsymbol{\theta}} + \mathbf{B}\boldsymbol{\theta} = \mathbf{C}\mathbf{q} + \mathbf{D} \tag{1}$$

can in principle be derived for sequential finite element, finite difference, finite volume, and boundary element-based inverse methods (where the latter can only be used in linear problems), and where the system matrices **A**, **B**, **C**, and **D** are determined by the discretization method used. Once the standard form equation is obtained, the second step in Beck's approach requires explicit least squares-based minimization of an error measure, S, between computed and measured temperatures. Minimization then leads directly to a linear (or quasilinear) *matrix normal equation* in the unknown instantaneous surface flux distribution [1].

Although Beck's method of parabolizing the inverse problem via the standard form and matrix normal equations is well-studied, and while Beck et al. [1] have presented a specialized treatment appropriate to linear, one-dimensional problems in planar geometries (encompassing most of the discretization methods mentioned above), to the authors' knowledge, a detailed implementation appropriate to multidimensional nonlinear problems had not been reported prior the work in Ling et al. [12].

The advantages associated with Beck's approach are numerous:

i) The method is non-iterative, transforming the inverse problem into a hybrid initial value problem in which the initial condition is known and the instantaneous surface flux boundary condition is

sequentially estimated via the matrix normal equation, based on measured data. The method thus offers an efficient alternative to the relatively expensive iterative approaches that presently dominate the field (see, e.g., [2,4]).

ii) The sensitivity matrix, $\mathbf{X}^{(\mathbf{n+1})}$, which plays a central role in many IHCP solution algorithms [1,2,4], can be explicitly determined, where in the finite element-based approach, for example, matrix elements of $\mathbf{X}^{(\mathbf{n+1})}$ are formed using elements of the global mass and stiffness matrices as well as area integrals associated with the global force vector. (See below.) This feature, which follows as a consequence of having obtained an explicit standard form equation, circumvents expensive solution of boundary value problems governing $\mathbf{X}^{(\mathbf{n+1})}$ or numerical evaluation of the derivatives comprising $\mathbf{X}^{(\mathbf{n+1})}$ [2].

iii) As described by Beck et al. [1], the method can incorporate any of the discretization schemes mentioned above.

iv) As also noted by Beck [1] and as demonstrated by Ling et al. [12], the method can be formulated for application to nonlinear, multidimensional inverse problems. [Note, the method developed in [12] is a nonlinear, multidimensional formulation, but was applied to a linear, one-dimensional benchmark problem and to a nonlinear, one-dimensional experimental problem].

The purpose of the present study is to investigate a simple method for stabilizing solutions of parabolic inverse heat conduction problems. In particular, a modified form of Beck's sequential function specification method is proposed in which computational, experimental, and future time intervals are allowed to differ. The investigation is motivated by three principle questions.

(i) Preliminary results reported by Keanini [13] suggest that choosing the computational time step, Δt, larger than the sample interval, $\Delta\tau$, improves inverse solution stability. Under the typical circumstance where the sample interval is shorter than the characteristic thermal diffusion time scale, τ_D [between the heated surface and the thermal measurement location(s)], it is clear that due to diffusional time lag, Δt should be chosen larger than $\Delta\tau$. While Beck et al. [1] have demonstrated the stabilizing effects of increased computational time step size relative to τ_D (using equal computational, sample, and future time step sizes), a detailed examination of the potential stabilizing effects of increased computational step size relative to sample interval size apparently has not been undertaken.

(ii) Investigators using the sequential function specification method have, without apparent exception, obtained future temperatures at time intervals equal to the computational time step, Δt. Based on the simple notion that increased thermal information can be obtained (and solution stability thus improved) by incorporating future temperatures at the typically smaller experimental sample interval, we will also investigate the potentially stabilizing effect of this approach.

iii) The method developed by Ling et al. [12], while providing a general finite element-based formulation of Beck's two-step strategy, in effect used exact matching of computed and measured temperatures. Since exact matching is prone to solution instability [1,4], a simple, non-iterative, stand-alone method for enhancing solution stability was sought. Although Tikhonov regularization [3] superficially meets these criteria, the method in fact requires a priori specification of both the regularization parameter and the form of the regularization term. By contrast, it appears that a modified function specification approach in which future temperatures are obtained at the relatively short experimental sample interval provides an objective, physically-based alternative to Tikhonov regularization. Specifically, the standard assumption [1] that the surface flux remains constant over the total future time interval, $R\Delta t_f$, is likely well met for small to moderate R since on this time scale (which is on the order of the measurements' temporal resolution), the detectable flux *does* remain essentially constant. (Here, R is the number of future times and Δt_f is the future time interval).

In overview, the FEM-based algorithm developed in [12] is first briefly described, with formulation of the standard form equation highlighted; a description of the solution, experimental, and future time intervals is given in the course of this development. Using the proposed modified function specification method, the associated matrix normal equation is then derived. The method is then validated against three well known example problems, designed respectively to test the ability of the technique to reconstruct rapidly changing surface fluxes, adapt to data truncation error and measurement error, and to solve nonlinear problems. Once validated, the technique is used to investigate surface heat transfer during experimental quenching of circular cylinders.

2 Inverse method formulation

2.1 Standard form equation

The initial-boundary value problem governing conductive heat transfer in the region of interest, Ω, is given by:

$$\nabla \cdot (k\nabla\theta) = \rho c \frac{\partial \theta}{\partial t}, \tag{2}$$

subject to the boundary conditions

$$\theta = \theta_\infty \qquad \text{on } \Gamma_1 \tag{3}$$

and

$$k\nabla\theta \cdot \mathbf{n} = q \qquad \text{on } \Gamma_2, \tag{4}$$

where Ω is bounded by $\Gamma = \Gamma_1 \cup \Gamma_2$, and where Γ_1 is the portion of the boundary subject to known temperature and/or heat flux conditions, and Γ_2 is the portion of the boundary on which thermal conditions are unknown. For simplicity, we assume that only temperatures are specified on Γ_1. The initial condition is

$$\theta(\mathbf{X}, 0) = \theta_0(\mathbf{X}), \tag{5}$$

where $\mathbf{X} = [x, y, z]$. In general, ρ, c and k are temperature-dependent, while q is dependent on time and space.

The direct problem defined by (2)– (5) is solved using the Galerkin finite element method, where the resulting system of equations is given by

$$(\mathbf{M} + \Delta t\mathbf{K})\boldsymbol{\theta}^{n+1} = \mathbf{M}\boldsymbol{\theta}^{n} + \Delta t\mathbf{f}^{n+1}, \tag{6}$$

and where components of the element capacity and stiffness matrices are given by

$$M_{ij}^{e} = \int_{\Omega_e} \rho c N_i N_j d\Omega \tag{7}$$

$$K_{ij}^{e} = \int_{\Omega_e} k N_{i,k} N_{j,k} d\Omega. \tag{8}$$

Note that Ω_e is the element area, N_i is a finite element interpolation function, and summation over k (= 1, 2, 3 for three-dimensional problems) is implied. Further, $\Delta t = t^{n+1} - t^{n}$ denotes the computational time step.

Here, the implicit, one-step, Euler backward-difference method is employed. It is important to note that in nonlinear problems where temperature variations are large enough to induce significant thermophysical property variations, quasilinearization [1] is used to evaluate $\mathbf{M}$ and $\mathbf{K}$. Thus, the magnitudes of ρ, c , and k at the current time step are evaluated using the temperature solution, $\boldsymbol{\theta}^{n}$, from the previous time step. In all cases, superscripts on $\mathbf{M}$ and $\mathbf{K}$ are suppressed for clarity. Components of the element force vector are given by

$$f_i^{e} = \int_{\Gamma_e} N_i q d\Gamma, \tag{9}$$

where Γ_e is the element boundary and where the time index has again been suppressed.

2.1.1 Computational, experimental, and future time steps

Prior to proceeding, it is necessary to define the various time steps and intervals that will be used in developing the standard form equation and inverse algorithm. In the development to follow, inverse solutions will be obtained at discrete times $t^{n+1} = (n+1)\Delta t$, where again Δt is the computational time step. In order to circumvent solution instability, the computational time step, $\Delta t = t^{n+1} - t^{n}$, is chosen to be larger than the experimental sample interval, $\Delta\tau$:

$$\Delta t = \beta\Delta\tau, \tag{10}$$

where β is a positive integer. As mentioned, this choice, dictated by the fact that $\Delta\tau$ is typically smaller than the characteristic thermal diffusion time scale, $\tau_D = L^2/\alpha$, allows for diffusional time lag between the surface Γ_2 and the sensors located at a characteristic depth L. [A minimum bound on the magnification factor, β, can be estimated by first recognizing that the computational time step must, at minimum, be on the order of τ_D, i.e., $\Delta t|_{min} \sim \tau_D$. Thus, $\beta_{min} = \Delta t|_{min}/\Delta\tau \sim \tau_D/\Delta\tau$; choosing values of β larger than β_{min} ensures that the computational time step is a larger-than-unity multiplier of the diffusion time scale].

Considering formation of the instantaneous least squares norm and subsequent formulation of the matrix normal equation (see Sect. 2.2 below), sets of measured and computed temperatures will be obtained at the current time, $t^{n+1}(= t^{(0)})$, and at R subsequent or *future* times, $t^{(1)}, t^{(2)}, \ldots, t^{(R)}$, where $t^{(m)}$ is related to t^{n+1} by

$$t^{(m)} = t^{n+1} + m\Delta\tau, \tag{11}$$

[As a point of comparison, the m^{th} future temperature in the standard approach is given by $t^{(m)} = t^{n+1} + m\Delta t$. Note too that while all of the data used in an inverse solution procedure is typically obtained prior to attempting a solution, in the special case where real-time or near real-time inverse solutions are sought, the computed solution at t^{n+1} must lag data acquisition by a time interval determined by the number of future measured temperatures used].

An illustration of the various time scales and intervals to be used is given in Fig. 1 for the case where $\beta = 2$ and $R = 4$.

2.1.2 Standard form equation

We now generalize our earlier approach [12] and express the global force vector at future time $t^{(m)}$ as

$$\mathbf{f}^{(m)} = \tilde{\mathbf{D}}\tilde{\mathbf{q}}^{n+1} + \mathbf{c}^{(m)}, \tag{12}$$

where $\tilde{\mathbf{q}}^{n+1}$ is the vector of parameters describing the instantaneous global surface heat flux vector $\mathbf{q}^{\mathbf{n+1}}$ on Γ_2, $\mathbf{c}^{(\mathbf{m})}$ is a vector produced by condensation (as determined by the primary boundary conditions on Γ_1), and where elements of $\tilde{\mathbf{D}}$, given by

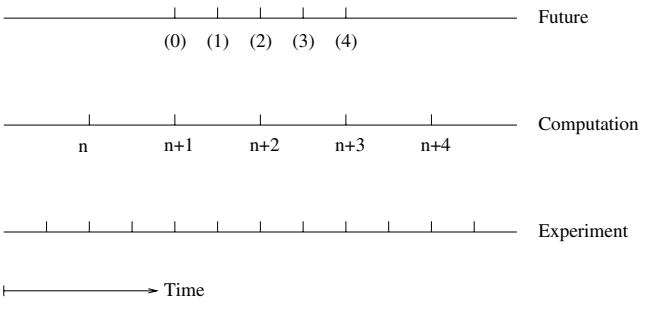

Fig. 1 An illustration of the time steps

$$\tilde{\mathbf{D}}_{Pk} = \frac{\partial f_P^{(m)}}{\partial \tilde{q}_k^{n+1}}, \tag{13}$$

are constants determined by the finite element discretization. See [12] for further details. Eq. (12) is of central importance in our development since it allows derivation of the linear matrix normal equation in $\tilde{\mathbf{q}}^{n+1}$. Indeed, Eq. (12) represents the finite element embodiment of Beck's function specification method [1] where, in the present case, the unknown flux at R future times is temporarily set equal to the flux at t^{n+1}. Note, in Eq. (13) that the upper case subscript P refers to a global node number, while the lower case subscript k refers to the local index over the K members of $\tilde{\mathbf{q}}^{n+1}$. (See [12] for further details.)

The explicit, FEM-based standard form equation, appropriate for use in the modified function specification scheme, is finally obtained by inverting the governing Eq. (6), i.e.,

$$\boldsymbol{\theta}^{(m)} = \mathbf{U}^{(m)}\mathbf{M}\boldsymbol{\theta}^n + \Delta t^{(m)}\mathbf{U}^{(m)}\mathbf{f}^{(m)} \tag{14}$$

where $\mathbf{U}^{(m)} = [\mathbf{M} + \Delta t^{(m)}\mathbf{K}]^{-1}$, $\mathbf{f}^{(\mathbf{m})}$ is given by (12), and where $\Delta t^{(m)} = t^{(m)} - t^n$. In our case, $\Delta t^{(m)} = \Delta t + m\Delta\tau$.

2.2 Matrix normal equation

Having obtained the standard form equation, we can now derive the associated matrix normal equation. The unknown instantaneous flux distribution, parameterized by the vector $\tilde{\mathbf{q}}^{n+1}$, is determined by first minimizing an instantaneous least squares norm, S^{n+1}, with respect to $\tilde{\mathbf{q}}^{n+1}$, where S^{n+1} is given by

$$S^{n+1} = \sum_{m=0}^{R}\left(\tilde{\mathbf{Y}}^{(m)} - \tilde{\boldsymbol{\theta}}^{(m)}\right)^T\left(\tilde{\mathbf{Y}}^{(m)} - \tilde{\boldsymbol{\theta}}^{(m)}\right). \tag{15}$$

Here, $\tilde{\mathbf{Y}}^{(m)}$ and $\tilde{\boldsymbol{\theta}}^{(m)}$ denote respectively, sets of measured and computed temperatures, obtained at corresponding locations within the body, at time $t^{(m)}$. The set of computed measurement site temperatures, $\boldsymbol{\theta}^{(m)}$, follow from (14):

$$\tilde{\boldsymbol{\theta}}^{(m)} = \tilde{\mathbf{U}}^{(m)}\mathbf{M}\boldsymbol{\theta}^n + \Delta t^{(m)}\tilde{\mathbf{U}}^{(m)}\mathbf{f}^{(m)} \tag{16}$$

where elements of $\tilde{\mathbf{U}}^{(m)}$ are related to those in $\mathbf{U}^{(m)}$ by $\tilde{U}_{iP}^{(m)} = U_{GP}^{(m)}$, and where the local index i (spanning the I measurement sites) maps to the corresponding global node G. Note that the reduced matrix $\tilde{\mathbf{U}}$ is of dimension $I \times N$. We again emphasize that although $\tilde{\mathbf{Y}}^{(m)}$ and $\tilde{\boldsymbol{\theta}}^{(m)}$ are generally obtained at time intervals equal to Δt [1], we obtain these sets at the shorter experimental measurement interval, $\Delta\tau$.

Minimization of Eq. (15) with respect to the members of $\tilde{\mathbf{q}}^{n+1}$ leads to

$$\sum_{m=0}^{R}[\tilde{\mathbf{X}}^{(m)}]^T[\tilde{\mathbf{Y}}^{(m)} - \tilde{\boldsymbol{\theta}}^{(m)}] = 0 \tag{17}$$

where $\tilde{\mathbf{X}}^{(m)}$ is the sensitivity matrix of dimension $I \times K$, and where elements of $\tilde{\mathbf{X}}^{(m)}$, given by

$$\tilde{\mathbf{X}}_{ik}^{(m)} = \frac{\partial \tilde{\theta}_i^{(m)}}{\partial \tilde{q}_k^{n+1}}, \tag{18}$$

represent the temperature response at measurement site i and time $t^{(m)}$ with respect to the k^{th} instantaneous heat flux parameter on Γ_2.

Given (18), (12) and (16), we first express the sensitivity matrix, $\tilde{X}^{(m)}$, in explicit form:

$$\tilde{X}^{(m)} = \Delta t^{(m)}\tilde{\mathbf{U}}^{(m)}\tilde{\mathbf{D}} \tag{19}$$

Finally, introducing (16) and (19) into (17), we obtain the linear matrix normal equation in $\tilde{\mathbf{q}}^{n+1}$:

$$\left(\sum_{m=0}^{R}\tilde{\mathbf{X}}^{(m)^T}\tilde{\mathbf{X}}^{(m)}\right)\tilde{\mathbf{q}}^{n+1} + \sum_{m=0}^{R}\tilde{\mathbf{X}}^{(m)^T} \times \left(\tilde{\mathbf{U}}^{(m)}\mathbf{M}\boldsymbol{\theta}^n + \mathbf{g}^{(m)} - \tilde{\mathbf{Y}}^{(m)}\right) = \mathbf{0}, \tag{20}$$

where $\mathbf{g}^{(m)} = \Delta t^{(m)}\tilde{\mathbf{U}}^{(m)}\mathbf{c}^{(m)}$. This important result, extending the method developed in [12], represents the finite element-based matrix normal equation, stabilized via the modified function specification method (where the version in [12] is obtained by setting $R = 0$ in Eq. (20)).

2.3 Inverse algorithm

Based on the preceding development, an algorithm for the inverse solution is proposed as shown in Table 1.

Refer to [12] for further discussion and a detailed illustration of the basic algorithm.

3 Validation tests

In this section, the above developed inverse method is validated against three example problems originally proposed by Beck [1, 14,15]. In all three problems, a flat plate heated at $x = 0$ and insulated at $x = L$ is considered. In the first problem, a surface heat flux is imposed at $x = 0$ and $t = 0$, and is then maintained constant in time. In the second case, the heat-flux is assumed to vary with time in a triangular fashion. The third case is similar to the first with the exception that thermal conductivity and specific heat are taken to be functions of temperature, thus making the problem nonlinear.

Exact solutions for all three problems are used to simulate experimental data. The performance of the proposed algorithm is then examined, and the results compared against those predicted by Beck's analyses. For purposes of comparison with Beck's results, we use

Table 1 Proposed inverse algorithm

Given $\boldsymbol{\theta}^n, \tilde{\mathbf{Y}}^{(m)}$, $\mathbf{M}$, $\mathbf{K}$, and $\mathbf{c}^{(m)}$:
1. determine $\tilde{\mathbf{q}}^{n+1}$ using Eq. (20);
2. calculate $\mathbf{f}^{n+1}(= \mathbf{f}^{(0)})$ using Eq. (12);
3. determine $\boldsymbol{\theta}^{n+1}(= \theta^{(0)})$ from Eq. (14);
4. increment the time index and return tostep (1).

nondimensional quantities in the discussion below. It should be noted that r, denoting the number of future times in Beck's work, is related to R, the number of future times in the present work, via the relation

$$(r-1)\beta = R \tag{21}$$

In other words, the time difference between the largest future time [which equals $R\Delta\tau$ here and $(r-1)\Delta t = (r-1)\beta\Delta\tau$ in Beck's work] and the current time, t^{n+1}, is the same in both approaches. In the comparisons to be described, the values of r reported by Beck will thus determine a corresponding value of R.

3.1 Case 1: Step change in surface heat flux at $x = 0$

The first case is designed to test the ability of the inverse method to reconstruct rapid changes in surface heat flux. Consider the flat plate shown in Fig. 2, where the plate, insulated at $x = L$, is subjected to a step-up in heat-flux from 0 to q_c, at $x = 0,\ t = 0$.

The exact solution in nondimensional terms is given by [1]:

$$\theta^+(x^+,t^+) = t^+ + \frac{1}{3} - x^+ + \frac{1}{2}(x^+)^2 - \frac{2}{\pi^2}\sum_{m=1}^{\infty}\frac{1}{m^2}e^{-m^2\pi^2 t^+}\cos(m\pi x^+) \tag{22}$$

where

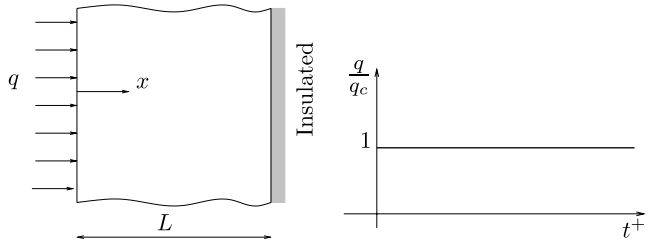

Fig. 2 Square insulated plate subjected to a step-up in heat-flux

$$\theta^+ = \frac{\theta-\theta_0}{q_c L/k}, \qquad t^+ = \frac{\alpha t}{L^2}, \qquad x^+ = \frac{x}{L}.$$

Here, θ_0 is the initial temperature, and k and α are the thermal conductivity and thermal diffusivity, respectively. Simulated noise-free experimental temperature data is generated from Eq. (22) at $x^+ = 1$ (corresponding to the insulated surface), at time intervals $\Delta\tau^+ = 0.01$. The nondimensional surface heat flux $\hat{q}^+ = q^n/q_c$, is then estimated (at $x = 0$) using two different computational time steps, $\Delta t^+ = 0.05$ and $= 0.5$, with the corresponding results shown in Figs. 3 and 4. For purposes of comparison, the results obtained by Beck et al. [1] using the standard function specification method in combination with a Duhamel integral solution of the direct problem are also shown.

Considering the results shown in Figs. 3 and 4, a number of observations can be made. Examining first the results obtained by exact matching of computed and experimental temperatures (R = 0; r = 1) [1], we see that the estimated flux obtained by the present method exhibits a large initial overshoot whose magnitude decreases with increasing step size, Δt^+. This feature can be explained as follows. When Δt^+ is small, the dimensional time increment Δt is much smaller than the diffusive time scale ($\tau_D = L^2/\alpha$); the initial temperature response at $t^+ = \Delta t^+$ and $x^+ = 1$ is thus suppressed and the corresponding predicted heat flux, $q^+(\Delta t^+)$, underestimated. At the next time step ($t^+ = 2\Delta t^+$), however, the temperature response (at $x^+ = 1$) increases, so that due to both energy conservation and the underestimated flux at $t^+ = \Delta t^+$, the corresponding flux estimate overshoots the actual value. This process of energy conservation-driven compensation for under- and over-estimated surface heat fluxes continues until the estimated flux begins to approach the actual value. The magnitude of the overshoot decreases with increasing Δt^+ due to an increasing initial temperature response at $t^+ = \Delta t^+$ and $x^+ = 1$. In contrast, the solution obtained by the standard function specification approach (using $\Delta t^+ = 0.05$) becomes unbounded soon after the initiation of heating. As discussed by Beck et al. [1], this result reflects a combination of solution sensitivity to exact matching

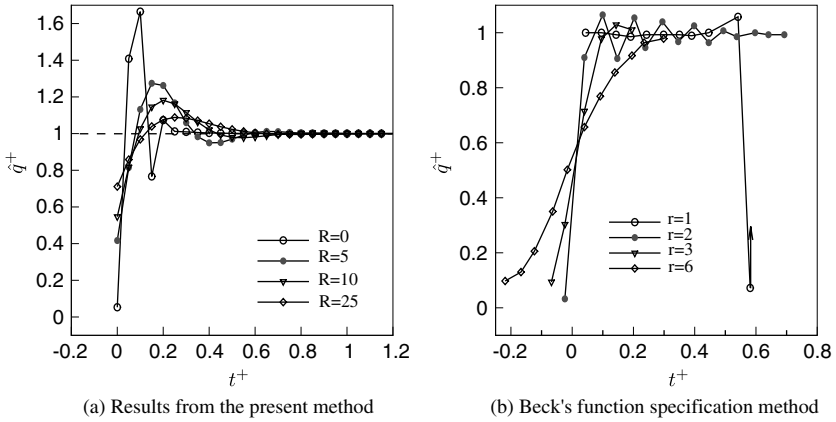

(a) Results from the present method (b) Beck's function specification method

Fig. 3 Calculated surface heat flux for constant q_c input to a plate. Exact temperature data, $\Delta t^+ = 0.05$, $\beta = 5$

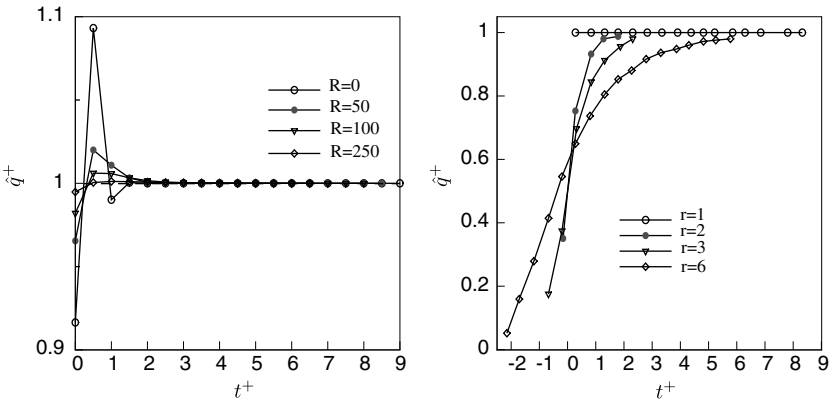

(a) The Present Method (b) Beck's function specification method

Fig. 4 Calculated surface heat flux for constant q_c input to a plate. Exact temperature data, $\Delta t^+ = 0.5$, $\beta = 50$

between the solution and data, and use of a time step that is too small relative to τ_D. Note that Beck's single future time step solution (r = 1), which in reality corresponds to Stolz's solution [1, 16], stabilizes at the larger time step, $\Delta t^+ = 0.5$.

The effect of adding future temperatures is apparent in Figs. 3 and 4 - both sets of solutions become smoother as R and r are increased. Notice, however, that while the solutions obtained by the present method rapidly approach the exact solution for both time steps and at all values of R, Beck's solutions, particularly those using $\Delta t^+ = 0.5$, exhibit early-time damping, an effect that becomes increasingly pronounced and extended as r increases. [Here, damping refers to estimates that remain less than the actual value.] Scale analysis of the matrix normal Eq. (20), expressed in the abbreviated form $\mathbf{A}\tilde{\mathbf{q}}^{n+1} = \mathbf{b}$, reveals the cause of overdamping: at early fixed times, the ratio $\|\mathbf{b}\|/\|\mathbf{A}\|$, indicating the approximate magnitude of $\tilde{\mathbf{q}}^{n+1}$, becomes smaller with increasing r. Importantly, based on the results in Figs. 3 and 4, we observe that the modified function specification method provides improved stability and reduced over-damping compared to the standard approach. Note finally the intuitively reasonable result that for both methods, early-time resolution of the unknown surface flux decreases with increasing time step size, Δt^+.

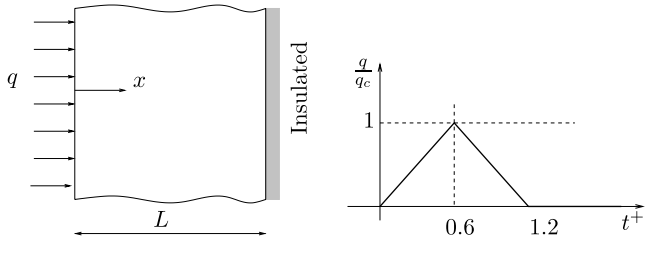

Fig. 5 Square plate subjected to a constant heat-flux and insulated at the other end

3.2 Case 2: Triangular surface heat flux at $x = 0$

The second test case, designed to assess the inverse method's performance when subjected to data truncation error [14] and random measurement error [1], is shown in Fig. 5. The insulated plate is subjected to a triangular heat flux at $x^+ = 0$, with the exact solution given in [1]. Temperatures obtained from the solution at the insulated end at nondimensional time intervals of 0.02 are again taken to be the exact experimental temperature data.

Considering first the effects of data truncation error, we follow Beck [14] and simulate this type of error by truncating the exact solution after the third decimal place. Specifically, using the measurement time interval $\Delta\tau^+ = 0.02$, we set the nondimensional temperature at $x^+ = 1$ equal to 0.000 for $t^+ = 0.02 * i$, $i = 1, 2, \ldots, 7$, and equal to 0.001 for $t^+ = 0.16$. Exact temperatures at subsequent time intervals are then truncated to three

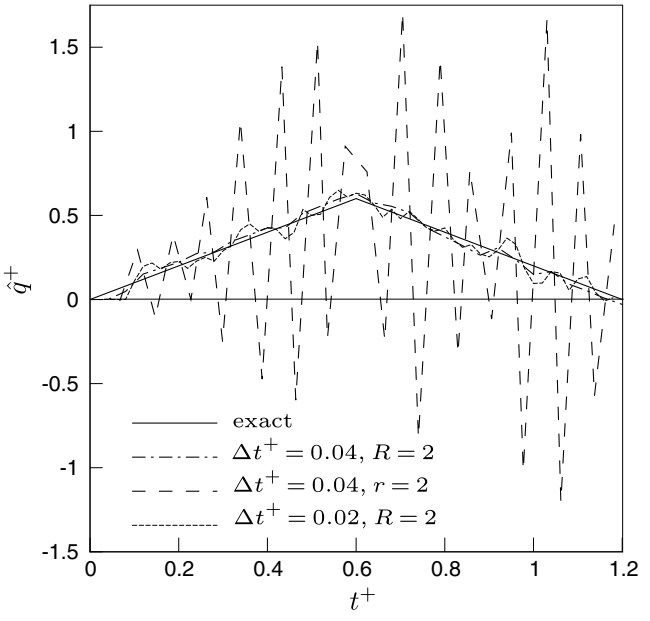

Fig. 6 Calculated heat flux for case 2 with measurement errors introduced by truncation of the exact temperatures. $\Delta\tau^+ = 0.02$

decimal places. Compared with actual temperatures, experimental temperatures for $t^+ \leq 0.16$ are in error by as much as 100%.

The surface heat flux at $x^+ = 0$, predicted by the present method and also by Beck's analysis [14], are shown in Fig. 6. The results correspond to the case when two future temperatures are used ($R = r = 2$), with $\Delta t^+ = 0.04$. [For convenience, we follow Beck [1] and refer to current temperatures, corresponding to $r = 1$, as future temperatures]. It is clear from the figure that the predictions generated by the present approach agree well with the exact solution, whereas Beck's solution ($r = 2$) exhibits significant instability. Predictions obtained by the present technique at a smaller computational time step, $\Delta t^+ = 0.02$, are also shown. For this time step, oscillations in the estimated flux become more pronounced, though still not as large as those accompanying Beck's solution. It is thus apparent that for this test case, data truncation errors do not significantly affect the algorithm's ability to accurately reconstruct the prescribed surface flux.

Computed surface temperatures at $x^+ = 0.0$, corresponding to the estimated fluxes in Fig. 6 (where $R = r = 2$), are shown in Fig. 7. Again, results obtained by the present method are in good agreement with the exact solution, and significantly less oscillatory than the predictions generated by the standard approach.

Although not shown, it is worth noting that the solution obtained by the present method using exact matching ($\Delta t^+ = 0.04$, $R = 0$) remains bounded, though oscillatory. However, the oscillations remain smaller than those accompanying Beck's two-future-time solution ($r = 2$, $\Delta t^+ = 0.04$). By contrast, the single-future-time solution ($r = 1$) becomes unbounded for $\Delta t^+ = 0.04$.

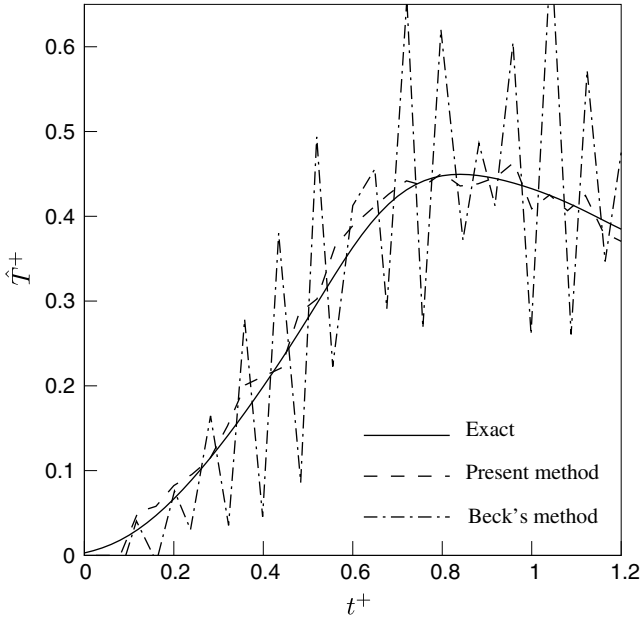

Fig. 7 Calculated surface temperature ($x^+ = 0$) using $R = r = 2$, $\Delta t^+ = 0.04$, and $\Delta \tau^+ = 0.02$

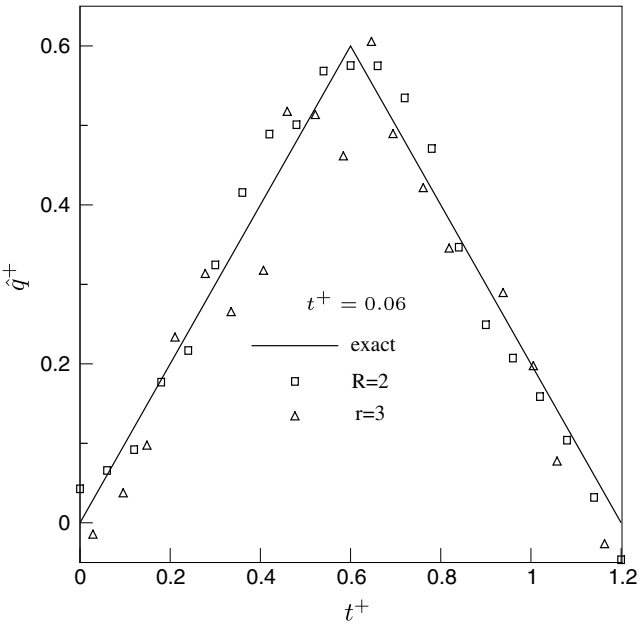

Fig. 8 Calculated heat flux for triangular heat flux with random error introduced into the simulated measurement data. $\Delta \tau^+ = 0.06$

Considering next the effects of measurement uncertainty, we follow Beck et al. [1] and use the same simulated random temperature signal that was used in their tests. In particular, simulated noisy temperature measurements, generated by adding a normally distributed random component to the exact solution at $x^+ = 1.0$ ($\Delta t^+ = 0.06$), are taken directly from Table 5.3 in [1]. The resulting surface heat flux estimates, corresponding to $\Delta t^+ = 0.06$, $R = 2$, and $r = 3$, are shown in Fig. 8. Close examination of the figure reveals that the solution obtained by the modified method is less oscillatory and somewhat more accurate than that obtained by the standard approach, particularly near the peak flux.

3.3 Case 3: Temperature dependent thermal properties

Here we consider a nonlinear problem studied by Beck et al. in [15]. As in the first example, a flat-plate, insulated at $x^+ = 1$, is subjected to a step-up in heat flux at $t^+ = 0$. However, the thermal conductivity and specific heat are now assumed to depend linearly on temperature according to

$$k = k_0(1 + a\theta) \qquad c = c_0(1 + a\theta). \tag{23}$$

where a is a constant, and k_0 and c_0 are the thermal conductivity and specific heat, respectively (evaluated at a reference temperature, θ_0); as given in [15], $k_o = 74.24\ \mathrm{Wm^{-1}K^{-1}}$, $c_o = 447\ \mathrm{Jkg^{-1}K^{-1}}$, and $a = 0.00086\ \mathrm{K^{-1}}$, representative of Armco iron at $\theta_o = 300$ K. Note, due to the use of the same temperature coefficient, a, in both property relationships in Eq. (24), these expressions are idealizations simply designed to capture the nonlinear effect produced by temperature-

dependent thermal properties [15]. Note too that there is no pre-specified limit on the temperature θ; as indicated by the exact solution to the corresponding linear problem, Eq. (22), and more to the point, as dictated by the physics of the problem, the temperature will continue rise with time, at least until the melting temperature is reached.

Using the Kirchoff transformation, defined by

$$u(x^+, t^+) = \int_0^{\theta} (1 + a\theta')d\theta' = \theta + a\frac{\theta^2}{2}, \tag{24}$$

the transient nonlinear heat conduction problem can be recast into a linear problem in the variable u [15]. The linear problem has a known exact solution that is identical to Eq. (22), with θ^+ replaced by $u(x^+, t^+)$.

The simulated measured temperature data is obtained at $x^+ = 0.1$ from the exact solution using $\Delta\tau^+ = 1.0$. Note that, unlike the previous two test problems, the sensor is located in the interior of the plate. The dimensionless time step is thus based on the distance, x_s, from the exposed surface to the sensor location; that is, $\Delta\tau^+ = \alpha\Delta\tau/x_s^2$.

In Fig. 9, the relative error between the estimated and actual heat flux is plotted against the time index. Again, an overshoot is seen at the beginning of the calculation. The solution then quickly converges to the exact value of unity, and for a time index up to 1000 (the largest tested), remains unchanged. As in example 1, it is also found that the initial overshoot can be considerably suppressed if a large number of future temperatures are used. Results obtained by the standard function specification method for a time index greater than 20 are not available. However, for a time index less than 20, the relative errors for both methods are found to be of the same order.

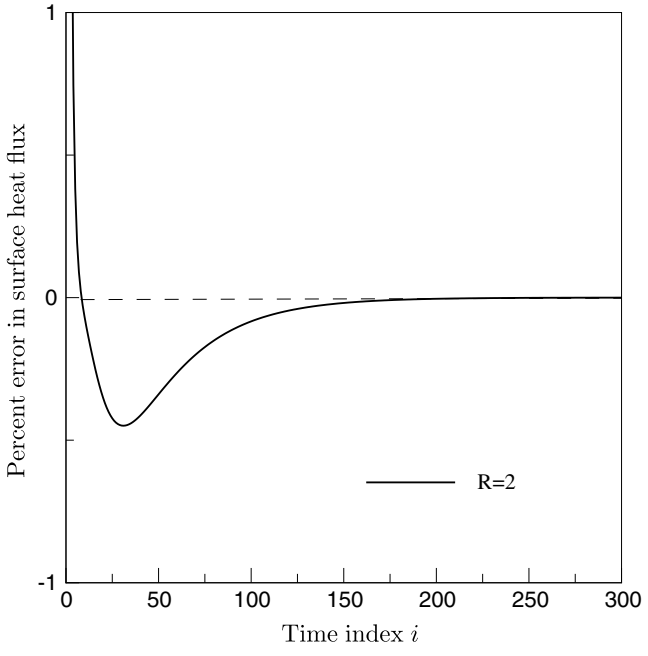

Fig. 9 Surface heat flux using exact temperature data when the material properties depend on temperature. $\Delta\tau^+ = 1.0$

4 Application to quenching problems

4.1 Experiments

Estimation of the surface heat flux during quenching of solid bodies represents a challenging task for inverse heat transfer algorithms. The nature of the heat transfer process at the interface between the quenchant and the part being quenched is extremely complex. For simplicity, the process can be conceptualized as occurring in three stages. In the initial stage when the part temperature is extremely high, a vapor blanket rapidly forms around the part. Depending on the part size, quenchant properties, latent heat of vaporization and ambient pressure, the blanket can persist or quickly collapse. Once the blanket collapses, heterogeneous, turbulent two-phase (nucleate boiling) heat transfer sets in (stage 2), and eventually gives way to single-phase natural convection (stage 3). The cumulative effect of these processes is a surface convective heat transfer coefficient that varies in a complex fashion with time.

In this section, we re-analyze the experiment reported in [12] where a metallic cylinder was quenched in oil and the associated interior temperature was measured in time. In particular, the proposed inverse method is used to estimate the time-varying surface heat flux from the cylinder. Surface heat flux predictions are then compared with analytical results due to Burggraf [17] and, as in [12], associated heat transfer coefficients are compared against those estimated by Bodin et al. [18] in an inverse analysis of a similar experiment.

The quenching experiments were performed using a Drayton Quenchalyzer [19]. As described in [12], an Inconel 600 metal cylinder, having a thermocouple at its geometric center, was heated in a furnace to a prespecified temperature, $\theta_0 = 850^oC$. See Fig. 10. Once a steady temperature was achieved, the cylinder was quickly transferred to a stagnant oil bath at $\theta_\infty = 40^oC$. Throughout, transient temperature changes at the center of the probe were acquired and stored by a computerized data acquisition system, sampling at a rate of 8 Hz ($\Delta\tau = 0.125$), for a period of 60 seconds. [Note that the thermal diffusion time scale, τ_D, between the surface and thermocouple was approximately 9.3 s.]

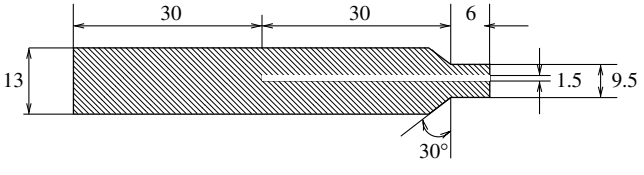

Fig. 10 A schematic of the probe used in experiments. All dimensions are in mm

4.2 Burggraf's analysis

Since the ratio of the probe's half length to its radius is around 5, it suffices to model the probe as a long solid cylinder and to neglect the influence of end heat fluxes. Thus, the problem reduces to finding the instantaneous surface heat flux for an infinitely long solid cylinder, where the temperature variation is only along the radius. Burggraf [17] presented one of the first analytic solutions to this problem using a series solution to the linear inverse problem. According to his solution, the heat flux is given by

$$q = k \sum_{m=1}^{\infty} \frac{m R_o^{2m-1}}{2^{2m-1}(m!)^2 \alpha^m} \frac{d^m Y}{dt^m}. \tag{26}$$

where Y is the surface temperature, and R_o is the radius of the cylinder. For computational purposes, the series is truncated at $m = 5$, derivatives are replaced by centered differences, and the time-varying temperature at the center of the cylinder is set equal to the experimentally observed temperature.

4.3 Results from the present method

Again, due to the probe's slenderness and relatively compact size, quenching is modeled as a one-dimensional axisymmetric problem. Fig. 11 shows the estimated surface heat flux when $\beta = 1$ and $R = 2$ ($\Delta t = \Delta\tau = 0.125s$). Also shown is the result from Burggraf's analysis where again, $\Delta t = 0.125$ s. It is seen from the figure that surface heat flux estimates from both methods are in excellent agreement.

Note that flux estimates become unbounded when no future temperatures ($R = 0$) are used (results not shown); the results presented correspond to the least stable solution obtained. It is also observed that stable solutions nearly identical to those given in Fig. 11 are obtained when $\beta = 2$ and $\beta = 5$, with $R = 1$ (results not shown). Due to the highly transient nature of surface heat transfer, use of more than one future temperature for $\beta > 1$ is found to produce solutions which lag somewhat behind the actual flux. Thus, a certain amount of trial and error may be required when determining R, particularly in strongly time-dependent problems.

The oscillations produced by the present method may in part reflect amplification of small amplitude, high frequency noise components in the measured temperature signal (note, these are not resolved in Fig. 12). As illustrated for example by Kurpisz and Nowak [4], estimated time rates of change of the surface flux vector $\mathbf{q}^{n+1}$ are subject to large amplitude variations due to time differentiation of the low amplitude, high frequency random component in the measured signal. An additional factor likely underlying the oscillatory flux estimates is associated with the fact that the computational time step, Δt, equals the experimental sample interval, $\Delta\tau$. As indicated by the results from the first test case above, Δt should be chosen larger than $\Delta\tau$.

Interestingly, the oscillating flux does not affect the accuracy of the estimated temperature at the center of the probe. As shown in Fig. 12, the estimated temperature history tracks the experimental history throughout. Due to the fact that both $\Delta\tau$ and Δt are much shorter than the thermal diffusion time scale, high frequency components in both the actual and estimated surface heat flux are smeared by diffusion. This results in smooth experimental and predicted temperature variations at the center (at least to the resolution of the plot). Comparing the temperature history obtained by the

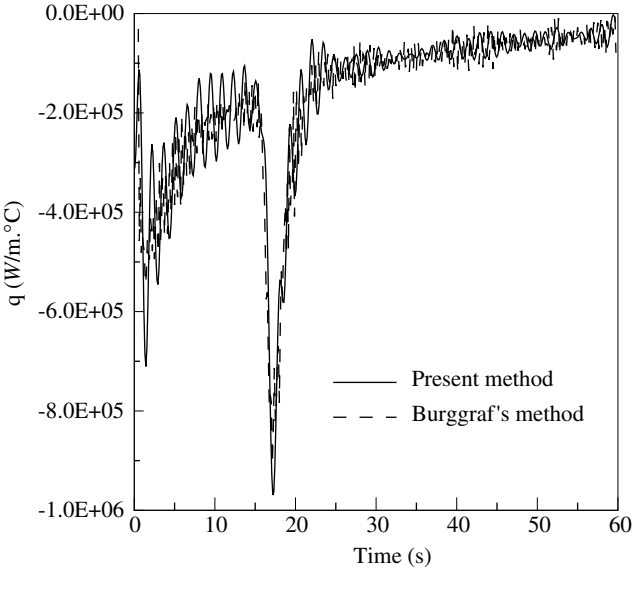

Fig. 11 Predicted surface heat flux as a function of time. For the present method, $\beta = 1$, and $R = 2$; for Burggraf's method, $\Delta t = 0.125$

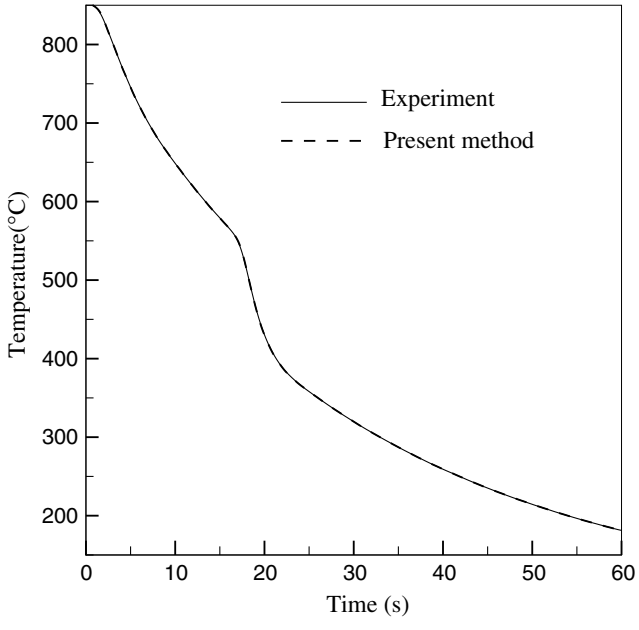

Fig. 12 Calculated center temperature using two future temperatures. $\beta = 1$

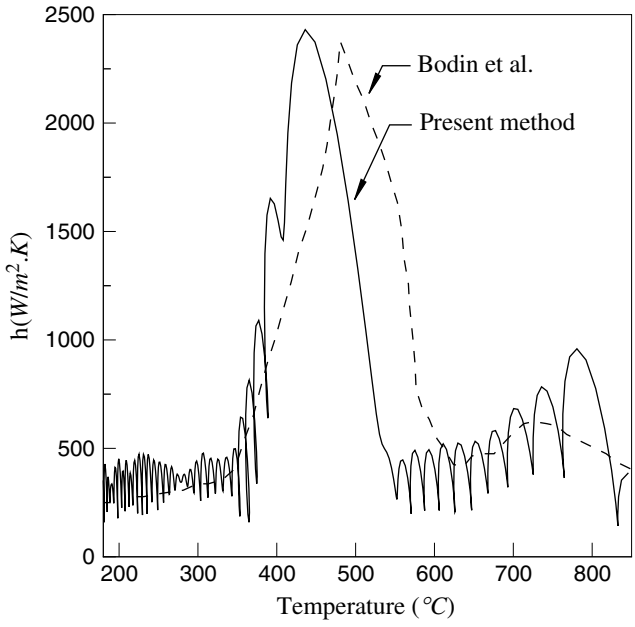

Fig. 13 Calculated heat transfer coefficients using two future temperatures. $\beta = 1$

present approach with that predicted via the non-stabilized method in [12], it is found that in the present case the maximum relative error between predicted and experimental temperatures is approximately 0.4%, roughly an order of magnitude smaller than the 3 to 5% maximum error observed in [12].

Heat transfer coefficients associated with the flux estimates in Fig. 11 are shown in Fig. 13 ($\beta = 1,\ R = 2$). Here,

$$h^{n+1} = \frac{q^{n+1}}{\theta_\infty - \theta_N^{n+1/2}}, \tag{26}$$

where $n+1$ again denotes the time index,

$$\theta_N^{n+1/2} = \frac{\theta_N^n + \theta_N^{n+1}}{2}, \tag{27}$$

and θ_N is the surface temperature. Also shown is a solution reported by Bodin et al. [18] who used a finite difference-based inverse method and an essentially identical experimental set-up. It is clear that solutions obtained by the present method are qualitatively and quantitatively consistent with those obtained by Bodin et al. [18]. Considering first the qualitative features exhibited in Fig. 13, the cylinder is initially enveloped in a vapor blanket over $850^oC \gtrsim \theta \gtrsim 560^oC$, with corresponding heat transfer coefficients remaining relatively small. The blanket then collapses, giving way to heterogeneous surface boiling and a rapid increase in surface heat transfer (beginning at $\theta \approx 560^oC$). Gradual suppression of two-phase heat transfer, reflected in the subsequent decay in h , occurs over $450^oC \gtrsim \theta \gtrsim 350^oC$. Finally, natural convection sets in over $350^oC \gtrsim \theta \gtrsim 180^oC$. Note that a similar interpretation holds for the estimated flux history in Fig. 11.

Quantitatively, a comparison of our results with Bodin's [18] shows that estimated h magnitudes during each stage of the quenching process are essentially equal. Moreover, maximum h values are also nearly equal. Although it appears that a significant offset exists between both estimates during the vapor collapse phase ($560\ C^o \gtrsim T \gtrsim 350\ C^o$), in reality, due to the violence and brevity of this process (occurring in less 10 seconds; see Fig. 11), it is likely that the offset merely reflects random variations in the degree of liquid-solid contact and nucleate boiling that occurs during collapse.

5 Summary and conclusions

A modified sequential function specification method has been developed for stabilizing solutions to parabolic inverse heat conduction problems. The method uses computational time steps that are larger than the typically short experimental sample interval, as well as future time steps that are equal to the sample interval. Beyond the advantages associated with Beck's two-step solution approach (detailed in Sect. 1), and in comparison to the standard function specification method in which the various time steps are set equal, the modified technique appears to provide: (i) more rapid error suppression and less damping of early time inverse estimates (under dynamic heat transfer conditions), (ii) improved stability and accuracy under comparable levels of data truncation and thermal measurement error, and (iii) comparable performance in nonlinear problems.

Application of the inverse method to experimental quenching of a cylindrical probe yields an estimated flux history nearly identical to that obtained via Burggraf's method [17]. In addition, comparison with Bodin's [18] earlier finite difference-based inverse analysis of a similar experiment shows that both approaches lead to qualitatively and quantitatively similar time-varying heat transfer coefficient estimates.

The methods developed in this and an earlier study [12] provide a stable, non-iterative, FEM-based approach for solving linear and nonlinear, multidimensional inverse heat conduction problems. These features, combined with explicit determination of the sensitivity matrix, suggest that the technique may be useful in applications requiring rapid inverse solutions, e.g., thermally-based process control, and thermally-based imaging (reconstruction) of sub-surface phase boundaries [20]. In addition, the method may be adapted to inverse problems in other areas, such as inverse convection and inverse radiation. Ongoing work in our group has also extended the method to the relatively difficult two-dimensional problem of estimating time- and space-varying surface heat fluxes on two separate boundaries; the results of this work will soon be reported.

Finally, it is important to again note that the methods developed here and in [12], while emphasizing a finite element-based solution of the direct problem, can be readily adapted to any other numerical scheme [1]. As described in the Introduction, Beck's method [1] of parabolizing the inverse heat conduction problem is comprised of two essential elements: i) formulation of the standard form equation, relating the vector of unknown flux parameters to the instantaneous temperature field, and ii) derivation of the matrix normal equation governing the evolution of the unknown parameter vector. The coefficient matrices arising in each of these equations are determined by the numerical method used to solve the direct problem.

Acknowledgments This research was supported by the National Science Foundation under Grant No. DMI-9820880.

References

1. Beck JV, Blakwell B, St Clair CR (1985) Inverse Heat Condution: Ill-Posed Problems. Wiley, New York
2. Ozisik MN, Orlande HRB (2000) Inverse Heat Transfer. Taylor-Francis, New York
3. Tikhonov AN, Arsenin VY (1977) Solution of Ill-Posed Problems. V.H. Winston and Sons, Washington, DC
4. Kurpisz K, Nowak AJ (1995) Inverse Thermal Problems. Comput Mech Publications, Boston, MA
5. Hensel E (1991) Inverse Theory and Applications for Engineers. Prentice Hall, New Jersey
6 Murio DA (1993) The Mollification Method and the Numerical Solution of Ill-Posed Problems. Wiley, New York
7. Alifanov OM (1994) Inverse Heat Transfer Problems. Springer-Verlag, New York
8. Zabaras N, Woodbury K, Raynaud M (eds) (1993) Proceedings of the Ist International Conference on Inverse Problems in Engineering: Theory and Practice. ASME, New York
9. Delaunay D, Jarny Y, Woodbury K (eds) (1998) Proceedings of the 2nd International Conference on Inverse Problems in Engineering: Theory and Practice. ASME, New York
10. Woodbury KA (ed) (2000) Proceedings of the 3rd International Conference on Inverse Problems in Engineering: Theory and Practice. ASME, New York
11. Orlande HRB (ed) (2002) Proceedings of the 4th International Conference on Inverse Problems in Engineering: Theory and Practice. ASME, New York
12. Ling XW, Keanini RG, Cherukuri HP (2003) A non-iterative finite element method for inverse heat conduction problems. Int J Numer Methods in Eng. 56:1315–1334
13. Keanini RG (1998) Inverse estimation of surface heat flux distributions during high speed rolling using remote thermal measurements. Int J Heat and Mass Trans 41:275–285
14. Beck JV (1970) Nonlinear estimation applied to nonlinear inverse heat conduction problem. Int J Heat and Mass Trans 13:703–716
15. Beck JV, Litkouhi B, St.Clair CR (1982) Efficient sequential solution of the nonlinear inverse heat conduction problem. Nume Heat Trans 5:275–286
16. Stolz G (1960) Numerical solutions to an inverse problem of heat conduction for simple shapes. ASME J of Heat Trans 82:20–26
17. Burgrraf OR (1964) An exact solution of the inverse problem in heat conduction theory and applications. ASME J of Heat Trans 86:373–382
18. Bodin J, Segerberg S (1992) Benchmark testing of computer programs for determination of hardening performance. In: George E. Totten (ed) Quenching and Distortion Control. ASM Int
19. Quenchalyzer Manual (2000) Instruments & Technology, Inc
20. Keanini RG (1997) Review: reconstruction and control of phase boundaries during fusion welding. Trends in Heat and Mass Trans 3:139–145